CREEP DAMAGE AND FAILURE OF SEVERAL PM NICKEL BASE SUPERALLOYS

J.-M. Escamez and J. L. Strudel

Centre des Matériaux de l'Ecole des Mines de Paris, B.P. 87, 91003 Evry Cédex, France

ABSTRACT

The development of creep damage was studied at 650°C in three nickel base superalloys obtained by powder metallurgy (P.M). Results on circumferentially notched specimens were compared with observations on cylindrical specimens in order to evaluate the effect of triaxiality of the stress state. Cavities of submicron size and cracks were counted by SEM techniques ans densities distributions were mapped on longitudinal sections of specimens tested close to their creep life time.

All observable defects were located in grain boundaries. The alloy with the lowest creep ductility exhibited a wide distribution of fewer cavities but an appreciable number of cracks. The spatial distribution was confined to the most loaded section. In the ductile material, on the contrary, the size distribution of the cavities did not extend much beyond 0,3 μ until failure was reached. Cracks were few and did not appear until the last stages before rupture. Nucleation of new cavities within a wide vicinity of the most highly stressed section kept nucleating until failure.

In notched specimens the density of observed defects is must higher than in cylindrical samples. The final rupture is initiated in the bulk by a mechanism of nucleation and coalescence of cavities into a dominant crack. In cylindrical specimens, the terminal crack is always initiated on the surface and propagates intergranularly first and eventually by transgranular shear.

KEYWORDS

Creep damage, cavities and cracks, P M nickel base alloy, turbine disk material, circumferentially notched specimens.

INTRODUCTION

Theoretical models attempting to take into account the development of creep damage are usually concerned with elementary mechanisms on the atomic level. In order to bridge the gap between these models and the laws describing plastic flow and failure on a macroscopic scale detailed experimental data is needed on the spatial distribution of damage in the micron scale and its evolution with time when final failure is appoached.

The first observations on notched samples were made in pure metals and single phase alloys such as copper (NEEDHAM and GREENWOOD 1975, KELLY 1976) and aluminum (BAMPTON and RAJ 1982). More recently alloys hardened by precipitates have also been investigated. CANE (1981) described the effect of triaxiality on cavity growth in Cr-Mo steels and DYSON (1981, 1983) studied the case of some nickel base superalloys either under uniaxial or under multiaxial stress states and generally after prestraining the material at room temperature.

The aim of this work was to study the development of creep damage leading to failure under low temperature and high stress conditions (650°C and over 1000MPa for the main stress). Since nickel base superalloys are known to be sensitive to environnemental effects and to nucleation of cracks on foreign particles when manufactured by P.M., circumferencially notched specimens were used. As mentioned by CANE (1979) a further advantage of this shape is the beneficial effect of stress triaxiality on the density of cavities associated with the intrinsic features of the material, such as grain boundaries, large γ' precipitates or dislocation substructure.

EXPERIMENTAL TECHNIQUES

1 -Materials and microstructures :

Three different nickel base alloys with large γ' volume fractions were studied. They were manufactured by P M techniques : argon atomized and HIPed slightly below solvus temperature in order to preserve a fine grain size (9-10 ASTM). Their compositions are presented in table I : RENE 95 and MERL 76 are commercial alloys, while ME 85 is an experimental alloy whose composition is intermediate between that of the two others and that of IN 100.

ALLIAGE	Cr	Co	Mo	W	Al	Ti	Nb	Hf	C	GRAIN SIZE (ASTM)
MERL 76	12.5	18	3.3	-	4.9	4.5	1.8	0.7	0.026	9 - 10
RENE 95	13.5	8	3.5	3.5	3.5	2.5	3.5	-	0.06	7 - 8
ME 85	12	15	4	-	4.5	3.8	1.5	0.2	0.025	9 - 10

- MERL 76 : 1165°C/2H/A.C. + 760°C/4H/A.C. + 650°C/24H/A.C.
- RENÉ 95 : 1175°C/1H/A.C. + 1140°C/1H/O.Q. + 870°C/24H/A.C. + 650°C/24H/A.C.
- ME 85 : 1180°C/1H/A.C. + 760°C/16H/A.C. + 800°C/6H/A.C.

TABLE I : Chemical composition (wt.%) and heat treatments of the materials tested.

The microstructures of all materials appear to be quite similar and are characterized by the presence of two populations of γ' precipitates : large γ' precipitates several microns in size usually located along grain boundaries and a high density of smaller, roughly spherical γ' precipitates (0,1 μ diameter) which hardens the matrix

2 - Testing procedure :

Test pieces were cylindrical either smooth with 23 mm gauge length or notched. The stress concentration factor for the notched samples was chosen rather small $K_t \simeq 1.4$.

The loading rate of the notched samples were chosen very carefully for each material after the results of previous relaxation tests. The initial stress concentration on the outer radius of the notched specimen must be relaxed by plastic flow during the loading procedure before the final value of the nominal stress is reached in the smallest section. For RENE 95 the loading rate was 2 MPa/h for a nominal stress of 1180 MPa since this material exhibited the slowest relaxation behaviour. For MERL 76 and ME 85 they were respectively 7 MPa/h for a stress of 1150 MPa and also 7 MPa/h for 1250 MPa. On cylindrical specimens stresses between 970 and 1034 MPa were applied. All tests were carried out at 650°C.

3 - SEM Observations

Fracture surfaces and longitudinal sections of damaged specimens for various fractions of life time were observed by SEM on a Philips PSEM 501. Densities of cavities and cracks were measured on longitudinal sections after mechanical and electrolytic polishing in a 10 HCL - 90 Methanol solution at -15°C under 16 volts.

On notched specimens 10 zones, with an area of 12000 μm^2 were observed along the minimal section. Such observations schemes were repeated every 0.25 mm along the stress axis.

Cavities and cracks below micron size were observed and measured at a magnification of 5 k or 10 k, with a threshold of detectability of about 0,1μ. Various artefacts connected with this mode of observations: initial density of porosities or cracks (≤2% of the total number), enlargement of cavities during electropolishing, etc, have been discussed elsewhere (ESCAMEZ 1984).

RESULTS

1 - Fracture surfaces

of notched specimens : Aside from the final 45° conical shear surface usually located at the periphery of the test piece and occupying less that 20% of the total facture area, two distinct zones could be identified :

- an intergranular zone corresponding to the initiation and propagation of the main crack leading to rupture. For samples loaded faster than the relaxation rate could allow, the stress profile is not inverted near the surface and cracks are initiated there rather than in the bulk. They tend to propagate in a direction normal to the surface rather than normal to the axis of the sample. The intergranular character extends over areas limited to 25-30% of the total rupture surface. When the loading rate is compatible with a full inversion of the stress profile, intergranular cracks are nucleated in the bulk of the minimal section, develop normal to the main stress axis and spread over 80-90% of the rupture surface.

- an area with mainly transgranular shear and cleavage-like aspect which extends over 50-60% of the rupture surface for excessive loading rates and is inclined to the sample axis rather than normal. This zone shrinks in area and even disappears into the intergranular zone when the loading rate is reduced.

of smooth cylindrical specimens : Rupture surfaces in this case looked similar to those of notched specimens that had been loaded too rapidly. The intergranular zone extends at most to 20% of the fracture area and lies perpendicular to the surface. In RENE 95 interupted at $t/t_R = 0.7$ the main intergranular crack observed after fracture at room temperature occupies no more than 4% of the sample section. This is an indication that crack propagation is mainly intergranular during creep and may be affected by the environnement as observed by MENON (1976). The zone of rapid propagation on an inclined transgranular surface spreads over 50 to 70% of the rupture surface and terminates on the final shear cone.

2 - Quantitative observations on longitudinal sections

Most of the observations have been carried out on notched samples, slowly loaded and after various fractions of life time. Results for $t/t_R = 0.9$ and 1 only are presented here, histograms for other interrrupted tests are reported elsewhere (ESCAMEZ, 1984).

Density of defects across the minimal section : The distribution of defects observed along the radius just before rupture and after rupture is shown on fig 1 for the three materials. All of the observed damage appears in the grain boundary as cavities or cracks.

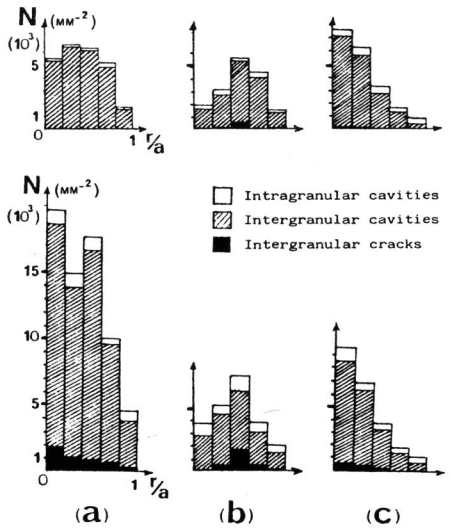

Fig 1 : Space distribution of damage across the minimal section in notched specimens for 0.9 t_R (above) and t_R(below) in MERL 76(a), RENE 95 (b) and ME 85 (c).

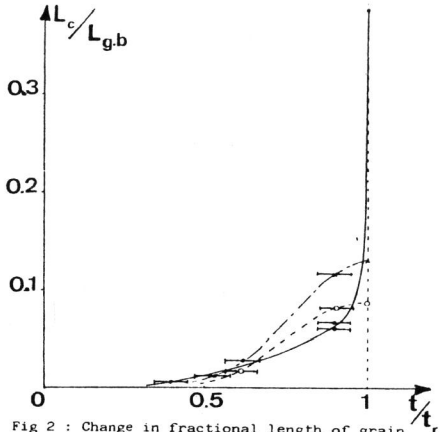

Fig 2 : Change in fractional length of grain boundary occupied by cavities versus creep time in MERL 76(——), RENE 95(— —) and ME85(– – –).

Alloy RENE 95 (fig 1b) shows a maximum density at half the radius with numerous cracks already open at $t/t_R = 0.9$ and the lowest average density of cavities of all three alloys. Alloy ME 85 (fig 1c) exhibits a cavity distribution centered on the axis of the sample. The highest distribution of defects is found in MERL 76 at rupture, with a profile centered around r/3 at 0.9 t_R and about the axis in the final stage. The improved ductility of this last alloy can thus be attributed to its ability to spread damage widely in the most stressed section. When considering the fractional length of grain boundary damaged during creep life (fig 2) alloy MERL 76 with its fine grain appears as the least affected at 0.9 t_R and RENE 95 as the most severely hurt. This situation is reversed during the final stage of creep life since MERL 76 has the ability to nucleate and develop cavities at an accelerated rate under high stress.

Density of defects along the stress axis O_Z : Quantitative results of SEM counts are mapped on fig 3 for the three alloys at 0.9 t_R. The decrease in damage density is fairly rapid : hardly any defects are observed beyond $z/a=0.45$ except for MERL 76 whose ability to generate cavities has already been mentioned. Damage is centered and spreads along the stress axis in ME 85, it is maximal at $r/2$ and confined along the O_Z direction in RENE 95 and it is widely spread in both r and O_Z direction but not centered in MERL 76. Cracks are not observed in MERL 76 but develop in areas of highest cavity densities in both ME 85 and RENE 95 with a concentration 3 times higher in the latter alloy.

Size distribution of cavities and cracks : Histograms in sizes of cavities averaged over the minimal section are presented on figure 4 for the 3 alloys at 0.9 t_R and t_R.

Almost all cavities are submicronic, 70 to 90% of them are smaller than 0.5 µm. Their density is inversely proportional to their size except for RENE 95 were they tend to grow to larger sizes at $t = 0.9\ t_R$. MERL 76 experiences a major growth of its cavities (50% on the average size) in the last 10% of its life time.

As for cracks : the size of the longuest crack observed after rupture is of the order of 15 µ for RENE 95 and ME 85 and 60 µ for MERL 76 which seems to withstand higher stress concentrations. Actually 80 to 90% of the cracks are shorter than 2 µ, so that their average size falls below this value.

The ability of an alloy to favor the development of cavities rather than cracks can be characterized by the ratio : crack length over total cavity length represented on figure 5. RENE 95 appears as crack prone and hence fragile, whereas the good ductility of MERL 76 is based on its ability to form cavities. ME 85 appears as a compromise alloy.

Shape orientation of cavities and cracks :

Cavities appear to be fairly equiaxed in both MERL 76 and ME 85 (fig 6a). They tend to link together in the last stages of the life time (fig 6b). In RENE 95, on the other hand, their shape is elongated along the grain boundary (fig 6c) and sharp edged cracks are already observed after 0.7 t_R.

Between 50 and 70% of all defects are located on grain boundaries quasi-normal to the principal stress axis and only 2 to 7% of the cavities in boundaries runnning parallel to it. Shape and orientations of defects do not seem to change with time or amount of strain.

Comparison with observations on smooth cylindrical samples

Longitudinal sections were polished and etched as before. Several areas were selected at random and quantitatively observed after rupture ($t=t_R$) but no systematic mapping of defects were attempted.

Cavities were similar in size, aspect ratio and location to those observed in notched samples but their densities were 3 to 20 times lower for respectively MERL 76 and RENE 95.

Internal cracks were even less frequent than cavities with densities divided by factors of 50 to 200 respectively for the same alloys. The density ratio (cracks/cavities) falls below 3% in smooth samples as compared to 10 to 25% in notched specimens (fig 1) and the average length is shortened by 60% : 0.9 µm instead of 1.8 µm.

Surface cracks on the outside of the samples, on the other hand, were present in large number. Their linear density could reach 30 mm/mm^2 in MERL 76 (with a g.b. linear density of 175 mm/mm^2) compared with 6 mm/mm^2 in RENE 95 (with a g.b. density of 85 mm/mm^2).

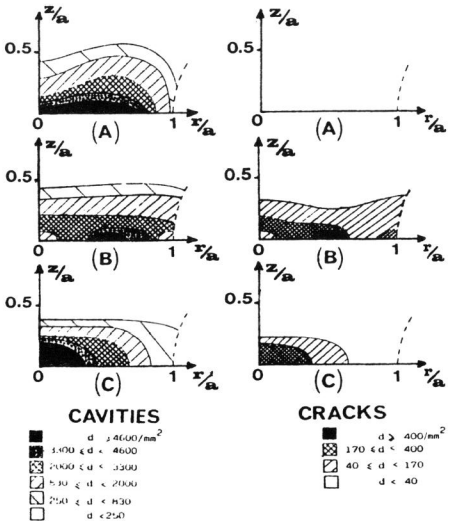

Fig 3 : Spatial isodistribution of cavities and cracks across minimum notch section and along maximum stress axis for $t/t_R = 0.9$ in MERL 76(A), RENE 95(B) and ME 85(C).

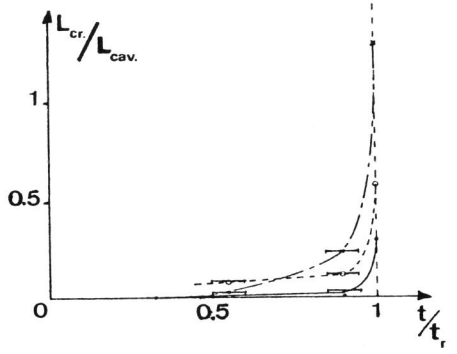

Fig 5 : Ratio of total crack length over cavity length versus creep time in MERL 76(——), RENE 95 (— –) and ME 85 (– – –).

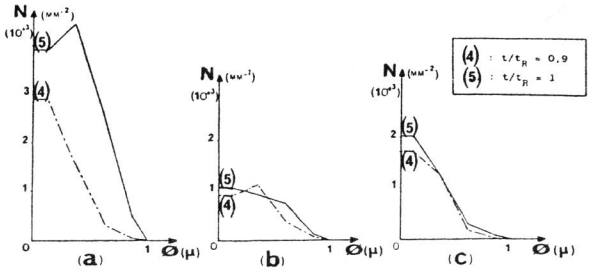

Fig 4 : Histograms of submicronic cavities for two different creep times in MERL 76(a), RENE 95(b) and ME 85(c).

DISCUSSION

It would be most interesting to compare the quantitative results of these observations with the stress or strain distributions in a notched sample, as calculated by a reliable model. HAYHURST et al (1977) used an elastic model combined with a steady state creep rate $\dot{\varepsilon} = A\sigma^n$ and examined the effect of the stress exponent. The stress profiles obtained with this model cannot explain the distribution of creep damage reported on figure 1. Loading the material above the yield point, resulting relaxation effects and various stages and shapes of creep curve for various materials cannot be taken into account on a simple model. A more complex model using the finite elements method has been developped (ESCAMEZ 1984) and provides a more reliable basis for interpreting some of the features of damage distribution. In accord with the previous observations made by LOVEDAY and DYSON (1979), the nucleation events are related to the amplitude of the principal stress σ_{ZZ} and the equivalent or Von Mises stress σ_e. The growth rate depends only on σ_e. For the shape of samples used here σ_e is almost constant across the minimal section os that growth is uniformly stimulated and the final cavity distribution follows quite closely the σ_{ZZ} distribution which varies significantly from one material to the other as observed experimentally (fig 1).

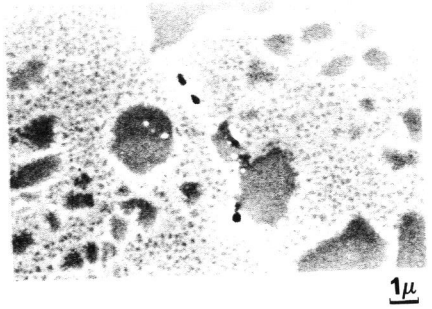

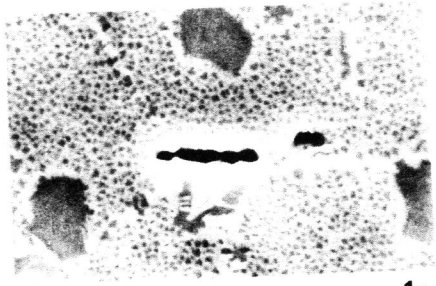

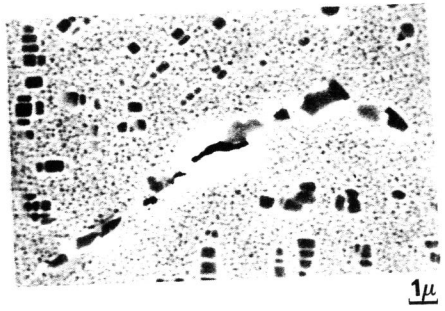

Fig 6 a : Isolated g.b. cavities in MERL 76 after creep

Fig 6 b : Linked cavities in ME 85 after crrep failure

Fig 6 c : Elongated cavities and cracks in RENE 95

CONCLUSIONS

In nickel base PM superalloys, creep damage at 650°C under about 1000 MPa in both circumferentially notched and in smooth specimens seems to develop in grain boundaries first as cavities and later as cracks.

When loaded slowly, notched samples are able to relax the outer stress concentration by plastic deformation and damage nucleates and grows in the bulk. In alloy RENE 95, the stress profile is only partially relaxed and maximum damage is located half way across the radius of the minimal section. In alloy ME 85 the stress profile is completely inverted and damage is maximum on the specimen axis. Alloy MERL 76 has the greatest ability to develop cavities in highly stressed regions, thereby

realizing critical load transfers and high ductility with case.

The average size of cavities is in the range 0.3 to 0.4 µm, that of cracks about 2 µm. Over 60% of all cavities and 90% of the cracks are located in grain boundaries normal to the main stress axis. They are much fewer and take on more elongated and acute shapes in RENE 95.

Linkage of intergranular cavities appears in the ultimate stages of creep life in ductile materials (MERL 76 and ME 85) and leads to the formation of rounded cracks. In brittle materials (RENE 95) cracks are already formed at 0.8 t_R. In both cases the fracture surface develops intergranularly during creep.

AKNOWLEDGEMENTS

This work was financially supported in part by SNECMA, in part by the Ecole Nationale Supérieure des Mines de Paris.

REFERENCES

BAMPTON, C.C. and RAJ, R. , 1982, Acta Met., 30, p. 2043 - 2053.
CANE, B.J., 1981, Met. Sci., 15, p. 302 - 310.
DYSON, B.F., 1981, "Creep and fracture of Engineering Materials and Structures" in B. WILSHIRE and D.R.J. OWEN (ed.), p. 235 -247.
DYSON, B.F., 1983, Script. Met., 17, p. 31 -37.
ESCAMEZ, J.M., 1984, Thesis : Microstructure and creep damage at 650°C in P.M. Nickel base superalloys.
HAYHURST, D.R. and HENDERSON, J.T., 1977, Int. J. Mech. Sci., 19, p 133 - 146.
KELLY, D.A., 1976, Met. Sci., 10, p 57 - 62.
LOVEDAY, M.S. and DYSON, B.F., 1979, ICM 3, 2, p. 213 - 222.
MENON, M.N., 1976, J. Mat. Sci., 11, p. 984 - 988.
NEEDHAM, N.G. and GREENWOOD, G.W., 1975, Met. Sci., 9, p 258 - 262.